Tidal Turbine Interaction Effect of Upstream Turbine Wake on Downstream Turbine

Vincent Podeur[*1], Dominic Groulx[*2], Christian Jochum[#3]

[*]*Department of Mechanical Engineering, Dalhousie University*
Halifax, Nova Scotia, B3H 4R2, Canada
[#]*Institut de Recherche Dupuy de Lôme (IRDL), ENSTA Bretagne*
Brest, FRE CNRS 3744, F-29200 Brest, France

[1]vincent.podeur@ensta-bretagne.org
[2]dominic.groulx@dal.ca
[3]christian.jochum@ensta-bretagne.fr

Abstract - **Flow perturbations carried in the wake of an upstream turbine can have a significant impact on the downstream one. To get a better understanding of the effect of unsteady asymmetric flow on a downstream turbine, fully transient simulations designed to study the effect of the wake of an upstream turbine on a downstream one were performed with a RANS *k*-ω SST turbulence model using ANSYS-CFX. Three different configurations were considered: the downstream turbine aligned with the upstream one, offset by 0.5*D*, and offset by 1*D*. A 10*D* clearance between both turbines was used. A horizontal axis tidal turbine (HATT) was used for the study. Results show that when fully in-line, the downstream turbine sees reduction in power coefficient by more than 69%, and temporal variation of this coefficient having a relative amplitude of more than 30%; and the blades see localized loading varying by a factor of up to 2 during their rotation and changes in the amplitude of loads applied at the same location varying by more than 13%.**

Keywords— **Horizontal Axis Tidal Turbine (HATT), Turbine Interaction, RANS-SST, Transient CFD, Blade Loading**

I. INTRODUCTION

A few full-scale turbines have been installed at various sites in Europe and northern America which all have been selected due to their high energetic potential. They all share, to some extends, similar characteristics linked to the nature of the tidal flow present. In fact, high velocity tidal currents are mostly observed in shallow coastal area, where narrowing channels occur in the topography and lead to flow acceleration. These area, with small water depth, may also be subjected to significant cycloidal motion in the flow induced by swells.

This harsh environment puts a lot of constrain regarding the design of tidal turbines and their implantation. One constrains of particular interest is the space limitation imposed by the topology of the local bathymetry. Contrary to what can be observed in the wind turbine industry, designer may not be able to position their turbines exactly the way they want, especially in the context of tidal turbine farms. Installing an array of turbines in such coastal area requires to take into account some key factors such as the impact of the farm on the local wildlife [1], its impact on the sediment transport or its effect on the local population activities (fishing for example). In addition to these limiting factors, operational and financial constrains should also be considered when designing a tidal farm layout, in order to reduce maintenance and installation costs [2].

In this context, two or more turbines may be installed in close proximity. This confinement is leading to unavoidable interactions between upstream turbines' wakes and downstream turbines [3]. The velocity deficit in conjunction with the increase of the flow turbulence will have an effect on the performance of the downstream turbine. Moreover, a downstream turbine situated partially in the wake of an upstream one would be exposed to an asymmetric flow which will induced asymmetric load on turbine blades.

As shown experimentally by Jeffcoate *et al.* [4], the high turbulence level of the incoming flow on a turbine has a significant impact on turbine performances, leading to a decrease of up to 63% of its performance (spacing between the turbines from 2*D* to 6*D*). This figure highlights the fact that perturbations carried in the wake of an upstream turbine may also be of significant impact on the downstream one.

This problematic has already been addressed but with simplified approaches such as the Blade Element Momentum Theory (BEMT) often coupled with a RANS CFD approach [5, 6]. These studies give interesting results regarding power extraction but as expressed in Leroux *et al.* [7], lack some precision regarding definition of the structure of the wake and its effect on load variation on the turbine blades.

To get a better understanding of the effect of unsteady asymmetric wake flow on a downstream turbine, fully transient simulation with RANS turbulence physics were run using ANSYS-CFX. Because of the proven relevance of the results obtained in earlier works [7-9], turbulent closure *k*-ω SST model has been used. Based on work previously done at Dalhousie University, simulations were designed to study the effect of the wake of an upstream turbine on a downstream one. Three different configurations have been considered: i) a downstream turbine aligned with the upstream one, ii) with an offset of half the turbine diameter (0.5*D*) with respect to the longitudinal axis on the right side of the upstream one, iii) with an offset of 1*D*. For all three setups, a 10*D* clearance between both turbines was used. The model of turbine considered for

this study is a horizontal axis tidal turbine (HATT), used by Doman *et al.* [10] and tested in the towing tank at the Kelvin hydrodynamics basin at Strathclyde University.

This paper will present the implementation of this model and the results of the numerical study. The problematic of assessing the quality of the wake from one turbine will be discussed followed by the question of upstream to downstream turbine interactions, including the predicted asymmetric load on the turbine blades for the three configurations studied.

II. Turbine Geometry

The turbine considered in this study is the one used by Doman *et al.* [10] and tested at Strathclyde University. The general dimensions of the turbine are given in Table I with a CAD rendering of it presented in Fig. 1. The blades are based on an NREL S814 profile, and for this study, blade roots were simplified to facilitate the meshing process. A much more detailed description of the blade geometry can be found in [8, 10] and will not be repeated here. Regarding the nacelle dimension, they were estimated from those papers.

III. Numerical Modelling

A. Fluid Domain and Boundaries Conditions

Two fluid domains have been investigated (see Fig. 2). They both share the same depth and width, which are based on the size of the Kelvin Hydrodynamics laboratory tow tank where the original turbine was tested, with a width of 4.6 m and a depth of 2.5 m; the length of both domains is different.

The first numerical domain contains one turbine and has a total length of 12D. Since the full recovery of the wake is not of primary interest in this study, for the sake of lowering the computing effort, a 10D length downstream of the turbine has been deemed sufficient. It is associated with an orthogonal reference frame $R_0(O, \vec{x}, \vec{y}, \vec{z})$. Its origin O is taken on the centreline of the channel at 2D from the inlet, with $\vec{z}$ pointing away from the inlet and $\vec{y}$ pointing upward. The turbine position, defined by the centre of its hub, is located at O, the origin of the reference frame.

The second numerical domain contains two turbines and has a total length of 17D. The same reference frame is considered as previously. The first turbine, referred as the upstream one, is located at the origin O. The second turbine, the downstream turbine, is at 10D on the z axis. Its y position is zero. For its x position, three setups are considered. A first one where the turbine is aligned with the upstream one. A second one with an offset of 0.5D on the x axis and a third one with an offset of 1D.

For both fluid domain, non-slip boundary conditions have been applied to the turbines and nacelles wall. For the sake of simplicity, free-slip conditions have been applied to the tank walls, those also mimic movement of the turbine assembly in a two tank better. These conditions are summed up in Table II.

B. Turbulence Model

Because of the proven relevance of the results obtained in earlier works [7, 8, 11-13], the Reynolds Average Navier-Stokes (RANS) with turbulent closure k-ω Shear Stress Transport (SST) model has been used. This two-equation eddy-viscosity model has been shown to properly account for turbulence in the free stream down to the viscous sublayer level close to the turbine walls [14]. This versatility is interesting since both turbine performance, which depends on the modelling of the boundary layers on its wall, and the wake which is in the free stream is of interest for this study

C. Computational Mesh

The computational domain is divided in two sub-domains. A rotating sub-domain, which encloses the rotating part of the tidal turbine and a stationary one which encloses the rotating sub-domain and the nacelle (see Fig. 3). Both domains are meshed separately using the ANSYS meshing tool. An unstructured meshing method using tetrahedral element is used. To ensure the continuity between both domain, the general grid interface (GGI) method is applied on all their shared boundaries. To achieve an accurate modelling of the wake, a cylindrical domain of refinement is added in the wake of the turbine, starting right after the centre of its hub. This cylindrical domain has a diameter of 1.5D.

TABLE I
Turbine Dimensions

Parameter	Dimension
Turbine diameter (D)	0.762 m
Hub diameter	0.15 m
Rotor depth	1.25 m
Nacelle length	1.70 m

TABLE II
Boundaries Conditions

Boundary	Condition
Inlet	Steady normal flow: $U_0 = 1$ m/s Turbulence Intensity = 5%
Outlet	Relative pressure $P_{rel} = 0$ Pa
Tank walls	Free slip, velocity at wall = U_0
Turbine walls	No slip
Nacelle walls	No slip

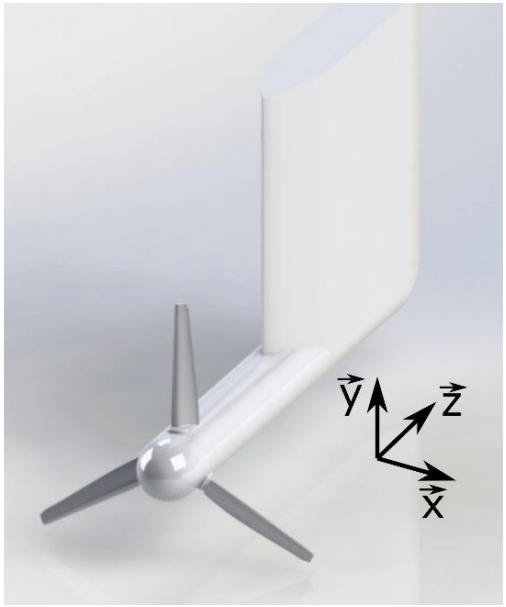

Figure 1 Turbine CAD rendering.

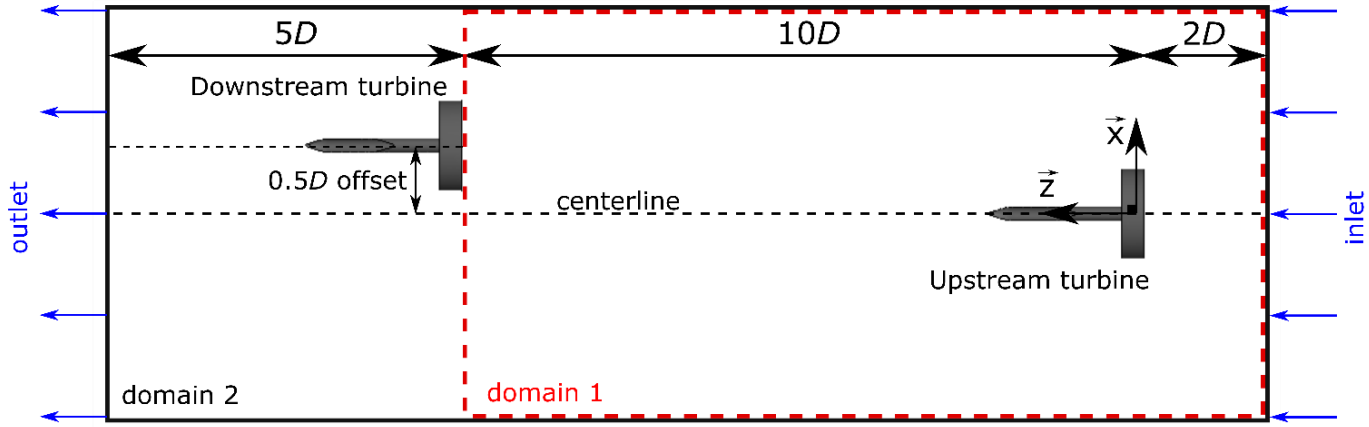

Figure 2 Fluid domains in the numerical studies.

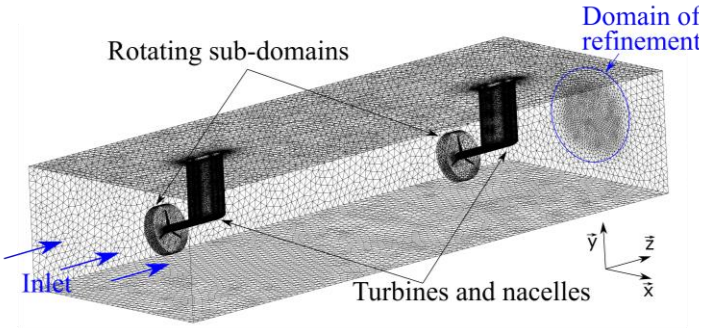

Figure 3 Meshed fluid domain.

D. Turbine Operation

For a single turbine in a uniform flow, simulations are performed at a given tip speed ratio (TSR); the turbine rotates at a rate that matches the TSR value for the given inlet flow velocity of 1 m/s in this work. Thus, a constant rotational speed is considered, and results are taken from the simulation once steady state, or quasi-steady state is reached; transient effects during the starting phase of the turbine while the flow velocity is increasing everywhere in the flow are not addressed.

For the two turbine simulations in a uniform inlet flow, the same approach is taken, the identical TSRs of both turbines are fixed, *i.e.*, both turbines rotate at a constant identical rotation rate. Looking specifically at the downstream turbine in this study, transient effect could occur when the turbine interacts with the non-uniform wake flow. Strong fluctuation in the flow may have a significant impact on the turbine dynamics by inducing torque variation; therefore, the rotation rate of the turbine could vary according to the inertia of the total system. Additional feedback loop to account for this fluid-structure aspect of the physics would be required, demanding additional computational resources. Such physical considerations were not accounted for in the simulations.

Finally, the transient simulations where performed on ANSYS CFX using a time step of 0.01 s for a total duration of 15 s (one turbine) and 20 s (two turbines).

IV. Mesh Quality Assessment

Extensive work regarding mesh refinement and results validation has already been carried out on this exact turbine at the Laboratory of Applied Multiphase Thermal Engineering (LAMTE) [8]. Therefore, the goal of the present work is not to go through the fastidious but necessary process of mesh convergence study again. Instead, this work will be used as a starting point and pushed further by switching from a qualitative description of grid convergence to a quantitative one. To do so, the work of P.J Roach [15], based on the Richardson extrapolation (RE) will be used. Such method is particularly relevant in the context of this study since no experimental data are available to validate the results from the simulation in the wake field. Thus, through its application, a better confidence of the numerical results can be gained.

A. Methodology

The method followed in this study is based on the one proposed in [16]. It is aimed at improving numerical work quality by making use of a standardised, well justified, method to report numerical uncertainty.

The grid convergence index (GCI) method, based on the RE, makes use of three significantly different mesh resolutions to evaluate the level of convergence reached by the mesh of interest. The GCI can be applied to an integral value, such as a thrust coefficient C_T or applied to a field variable like the velocity profile of the flow in the wake. This method has therefore been followed here and is described in detail hereafter.

First, a representative mesh size h is defined for all three meshes, Eq. (1):

$$h = \left[\frac{1}{N_{int}}\sum_{i=1}^{N_{int}}(\Delta V_i)\right]^{\frac{1}{3}} \quad (1)$$

with ΔV_i the volume of the ith cell and N the total number of cells in the volume of interest.

Then, the refinement factor between two consecutive meshes can be computed using Eq. (2):

$$r_{cm} = h_c/h_m \quad (2)$$

where h_c and h_m are the representative mesh sizes of the coarse and medium meshes respectively, and r_{cm} is the refinement factor between the coarse and medium meshes. This computation must also be done between the medium and fine meshes to get the factor r_{mf}. Then, the apparent order p of the method can be computed for every reference point using Eqs. (3) to (5).

$$p = \frac{1}{ln(r_{mf})}\left(ln(\epsilon_{cm}/\epsilon_{mf}) + ln\left(\frac{r_{mf}^{p} - s}{r_{cmf}^{p} - s}\right)\right) \quad (3)$$

$$s = 1 \times sgn(\epsilon_{cm}/\epsilon_{mf}) \quad (4)$$

$$\begin{aligned} \epsilon_{cm} &= \phi_c - \phi_m \\ \epsilon_{mf} &= \phi_m - \phi_f \end{aligned} \quad (5)$$

where ϕ_c, ϕ_m and ϕ_f are the variable of interest, stemming from the results of the coarse, medium and fine mesh simulations. Equation (3) can be solved with a simple iterative method. The extrapolated values can then be computed using Eq. (6):

$$\begin{aligned} \phi_{ext}^{mf} &= (r_{mf}^{p}\phi_f - \phi_m)/(r_{mf}^{p} - 1) \\ \phi_{ext}^{cm} &= (r_{cm}^{p}\phi_m - \phi_c)/(r_{cm}^{p} - 1) \end{aligned} \quad (6)$$

The approximate relative error between medium and fine meshes is then given by Eq. (7):

$$e_a^{mf} = \left|\frac{\phi_f - \phi_m}{\phi_f}\right| \quad (7)$$

and the extrapolated relative error by Eq. (8):

$$e_{ext}^{mf} = \left|\frac{\phi_{ext}^{mf} - \phi_f}{\phi_{ext}^{mf}}\right| \quad (8)$$

The medium mesh convergence index is given by Eq. (9):

$$GCI_m^{mf} = \frac{1.25e_a^{mf}}{r_{mf}^{p} - 1} r_{mf}^{p} \quad (9)$$

This method can then be used to evaluate the numerical uncertainty associated to the results from the medium mesh.

B. Turbine Performances Validation

The metrics considered for the validation are the power and thrust coefficients C_p and C_T.

$$C_p = \frac{\omega Q}{\frac{1}{2}\rho_w A U_0^3} \quad (10)$$

$$C_T = \frac{T}{\frac{1}{2}\rho_w A U_0^2} \quad (11)$$

where Q and T are the turbine torque and thrust respectively, ρ_w is the fresh water density taken as 995 kg/m^3, ω is the rotational rate in rad/s and A is the swept area in m^2 of the turbine and is given by Eq. (12). Is it important to note that both coefficients are evaluated for both turbines using the free-stream constant inlet velocity, even if the downstream turbine will see a disturbed flow having an average, and a local velocity, that will differ from the inlet value of U_0.

$$A = \pi\left(\frac{D}{2}\right)^2 \quad (12)$$

Transient simulations were performed for three tip speed ratio (TSR) values, as defined in Eq. (13).

$$TSR = \frac{\omega D}{2U_0} \quad (13)$$

Thus, by applying the GCI method presented before, numerical uncertainty can be evaluated and added to the results of the simulations.

The mesh quality assessment was performed using the single turbine model. For these simulations, the time step was set to 0.01 second with total simulation length of 15 seconds. This duration was enough to attain a well-established flow, where C_p and C_T coefficients reached steady state values. The results from the GCI method are provided in Table III for the three meshes used in this part of the study; the mesh refinement ratios for these meshes are provided in Table IV.

From Table IV, the mesh ratios are below the recommended value of 1.3 suggested in [16]; this value of 1.3 is based on practical experience. As expressed in [17], for non-integer grid refinement, a 10% change in the refinement process is the recommended minimum provided that the coarse grid is within the asymptotic range; the meshes selected in this study are also within this range. From Table III, it is interesting to notice that an oscillatory convergence is observed for C_p, with negative values of s. Regarding the GCI value for each TSR, it appears that the results are well converged. For C_p, all three values are below 1%. For C_T, the numerical uncertainty is slightly higher, with values between 1.71% and 0.46%.

Simulation results (C_p and C_T as a function of TSR for all three meshes) are given in Table V. These simulation results for the medium mesh are plotted along with the experimental results from Doman *et al.* [10] for comparison/validation in Fig. 4.

Figure 4 shows some discrepancies occurring between the numerical and experimental tow tank results. Even though numerical and tow tank results follow the same trend, turbine performances are slightly overestimated. The highest discrepancy was found at TSR 4.5 for C_P value, with a difference of 15%. The lowest discrepancy is for the C_T value at TSR 4.5 with a difference of 8% compared to the measurement.

This small difference between numerically predicted and experimental values can be explained by the simplification done during the modelling process of the turbine. To that point, Currie *et al.* [8] showed that minor changes to the blade geometry (especially the trailing edge) and slight difference in boundary layer meshing on the wall of the blades, could result in significant variation of the predicted values for both C_p and C_T.

Table III
Results from GCI Method

	p			s			e_a^{mf}			e_{ext}^{mf}			GCI_m^{mf} (%)		
TSR	3.5	4	4.5	3.5	4	4.5	3.5	4	4.5	3.5	4	4.5	3.5	4	4.5
C_P	13.47	15.48	20.38	-1	-1	-1	0.22	0.37	0.35	0.08	0.10	0.06	0.38	0.60	0.51
C_T	6.78	11.45	6.53	1	1	1	0.65	0.24	0.27	0.71	0.12	0.30	1.71	0.46	0.71

Table IV
Meshes Refinement Ratios

$r_{cm} = 1.1013$
$r_{mf} = 1.1356$

Table V
C_p and C_T Results as a Function of TSR for the Three Meshes Used

	TSR	Coarse	Medium	Fine
C_P	3.5	0.3122	0.3158	0.3151
C_T		0.4834	0.4746	0.4715
C_P	4	0.3127	0.3207	0.3195
C_T		0.4945	0.4886	0.4874
C_P	4.5	0.2945	0.3081	0.3070
C_T		0.4912	0.4876	0.4863

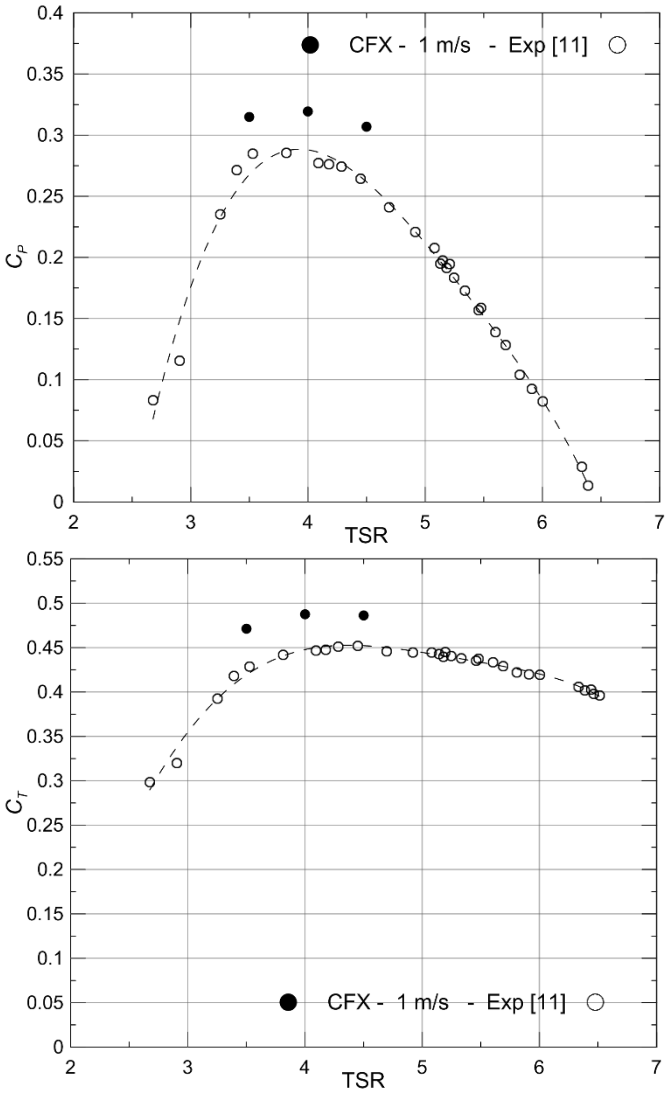

Figure 4 Numerical C_p and C_T as a function of TSR compared to experimental measurements from [10].

Additionally, some physical phenomenon, such as hydromechanical interaction between the flow and blades, inducing load variation, vibration, potential rotational speed variation and energy loss, are neglected. Therefore, the values obtained are considered to be satisfactory regarding the approximation made on the turbine geometry and the grid selection made to reduce the computational time.

C. Wake quality assessment

According to the authors research, little work has been carried on wake convergence and wake quality assessment. One of the classical approach for wake convergence analysis consists in a qualitative comparison of the results from the whole set of considered grids, for example through the use of velocity deficit downstream of the turbine. This is what is done in [18]. Despite giving some insight on the wake quality, this approach is limited to one-dimensional evaluation and does not provide any quantitative information regarding the convergence of the results. By following the method proposed in section A, it is possible to quantify the convergence of the results within the wake.

The wake structure is defined by the spatial evolution of a field variable which is the flow velocity along the z axis. Special care should be taken while applying the GCI method. Because a field variable is considered, the local cell size evolution should be considered when the refinement factors are computed. In order to ensure that the principle of significant change in the grid refinement process is respected; the GCI study in the wake covers only the cylindrical domain of refinement mentioned previously. Indeed, the cell size outside this virtual domain was not varying enough to ensure relevant results. Thus, the local cell size is given by evaluating the mean cell size in the virtual cylinder of refinement, between the 7D and the 10D locations in the turbine wake. The results of meshes ratios are given in Table VI; in this case, the ratios are well above the recommended 1.3.

Table VI
Wake Refinement Meshes Ratios

$r_{cm} = 3.6695$
$r_{mf} = 1.7901$

Table VII
Results from GCI Method in the Turbine Wake

Variable	Value
P_{mean}	1.2854
s	-1 → 26% 1 → 74%
$e_{a\ mean}^{mf}$	1.95%
$e_{ext\ mean}^{mf}$	4.56%
GCI_{mean}	8.60%

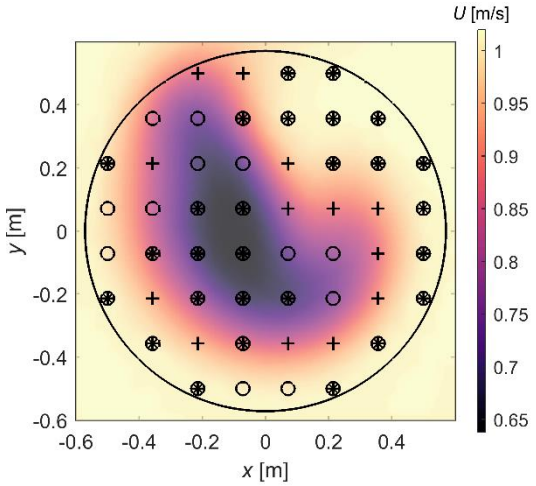

Figure 5 Contour plot of the velocity in *z* direction, 10*D* downstream of the turbine. ○ valid data, + invalid data, ● data below the mean GCI value.

Table VIII
Final Mesh Information

Global meshing parameter	
Number of elements	23,785,687
Min element size	2.75×10^{-4} m
Max face size	0.15 m
Curvature Normal angle	7.5°
Max Wake cell size	4.5×10^{-2} m
Boundary layer meshing parameter	
Number of layers	30
Max thickness Blades	1.5×10^{-2} m
Max thickness Blades roots	1.5×10^{-2} m
Max thickness Hub	3×10^{-2} m
Max thickness Nacelle	5×10^{-2} m

Because the mesh is unstructured, it is not possible to have coinciding computation points on each mesh. The work around is to define a finite number of points of interest in the bulk of the wake. In Fig. 5, the selected points are visible within the cylindrical domain represented by the circular line. There is a total number of 52 points. The spacing between each point in the *x* and *y* directions is 0.143 m. The GCI method was performed in the wake over those 52 points. The results of the calculation are given in Table VII. Over the 52 points of interest, GCI computation succeeded on 39 points. For the remaining 13 points, the computation failed or gave invalid results with GCI values over 100%. The reason for calculation failure was mainly due to values being too close between each meshes, which gave very small results in Eq. (5). This lead to failure in computing the value of *p*. It is worth noticing that almost 70% of the valid data points gave a GCI index lower than the mean value of 8.6%. Oscillatory convergence occurs 26% of the time (*s* value negative).

Regarding the distribution of the results over the data point locations, it can be observed in Fig. 5, that the valid data below the mean value of GCI are roughly located in the centre of the wake (where the main flow deficit occurs) and the outer flow.

By considering the trade-off to be made in order to keep the simulation time below a reasonable duration, it can be considered that a reasonable level of convergence in the wake is reached with a mean value of GCI below 10%. At this point, even if some details of the flow are fully well represented, it is safe to say that the bulk of the wake structure and its velocity profile are well represented at 10*D* downstream the first turbine.

Thus, reasonable trust can be put in the next step of the study which is to evaluate the impact of this wake on the downstream turbine performances and load variation. For the rest of this study, the converged mesh (the medium mesh from the previous discussion) having the properties listed in Table VIII is used.

V. Results and Discussion

A. Single Turbine Wake

Once a downstream turbine is added behind this one, its performances will strongly depend on the nature of the incoming flow in the wake. Figure 7 shows the flow velocity at cross-sections situated 3*D*, 7*D* and 10*D* in the wake of the turbine; remembering that the downstream turbine will sit a distance 10*D* in the wake of this one. From Fig. 6, it is clear that the flow is far from having recovered, with a minimum velocity at 10*D* of 0.65 m/s which is 65% of the inlet velocity. It is also observed that there is a substantial region, extending more than 0.2 m in all directions around the central point of the turbine hub where the velocity remains below 0.75 m/s or at level below 75% of the inlet velocity.

Outside the wake, the flow velocity sees a significant increase of 10% compared to the inlet velocity with a value of 1.1 m/s. This increase is the result of mass conservation and blockage effect, more so blockage from the turbine and nacelle, than the walls of the numerical domain.

Regarding the shape of the wake, a strong asymmetry can be noticed. Figure 7 points to the cause and mechanism behind this deformation of the wake. The two in-plane components *u* and *v* of the flow velocity are represented by tis vector field. A strong swirling occurs in the wake with in-plane velocity going up to $1/10^{th}$ of the inlet velocity. Two corotating vortices can be observed on Fig. 7. As expressed in [19], the strain field arising from their interaction tends to deform elliptically the structure of the vortex. This flow deformation evolves with respect to time while being advected in the wake, which leads to the stretched shape of the wake observed at 10*D* in Fig. 6.

Specifically, when it comes to the position of the downstream turbine at 10*D*, in this study, the turbine is placed to the right of the upstream turbine when looking at the assembly from the front. From Fig. 4, this means that the downstream turbine is placed on the side where the flow has recovered slightly more, but where the turbine blades will encounter a flow in the wake with velocities over a greater range, from 0.65 m/s to 1.1 m/s (the positions of the downstream turbine central hub in two of the studied configurations are shown with a green X on Fig. 6).

B. Downstream Turbine Performances

Simulations looking at the interaction of the downstream turbine with the wake generated by the upstream one were performed at a TSR = 4. This value was selected since it is within the range of maximum C_p values while happening at a slower rotation rate which enables greater temporal resolution without the need for much shorter numerical time steps.

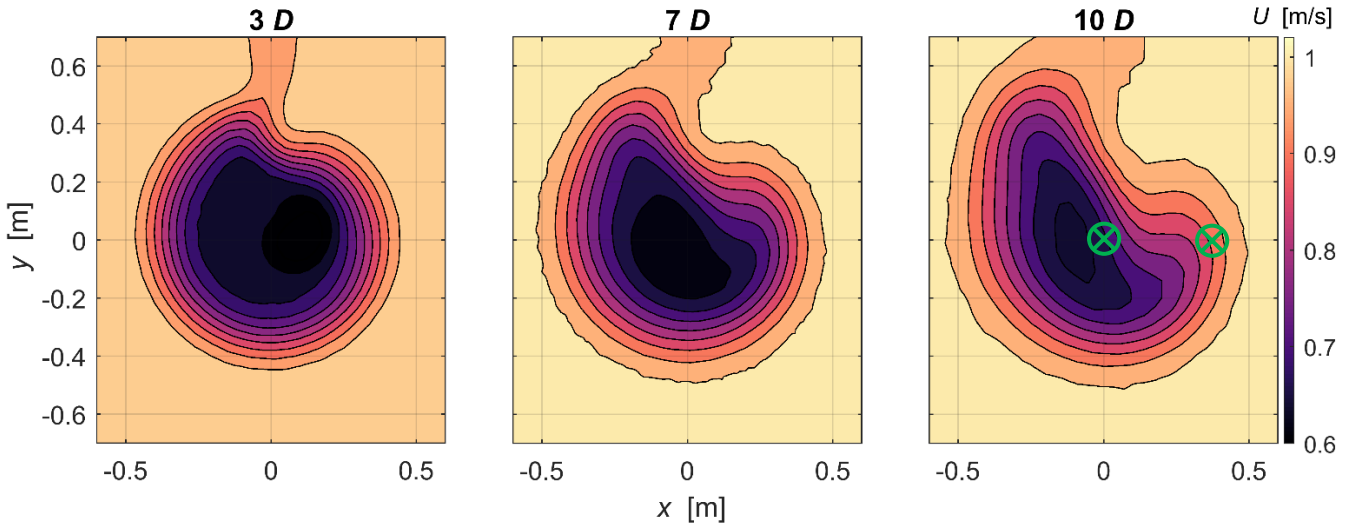

Figure 6 Wake velocity at cross-sections located 3*D*. 7*D* and 10*D* in the wake of the turbine.

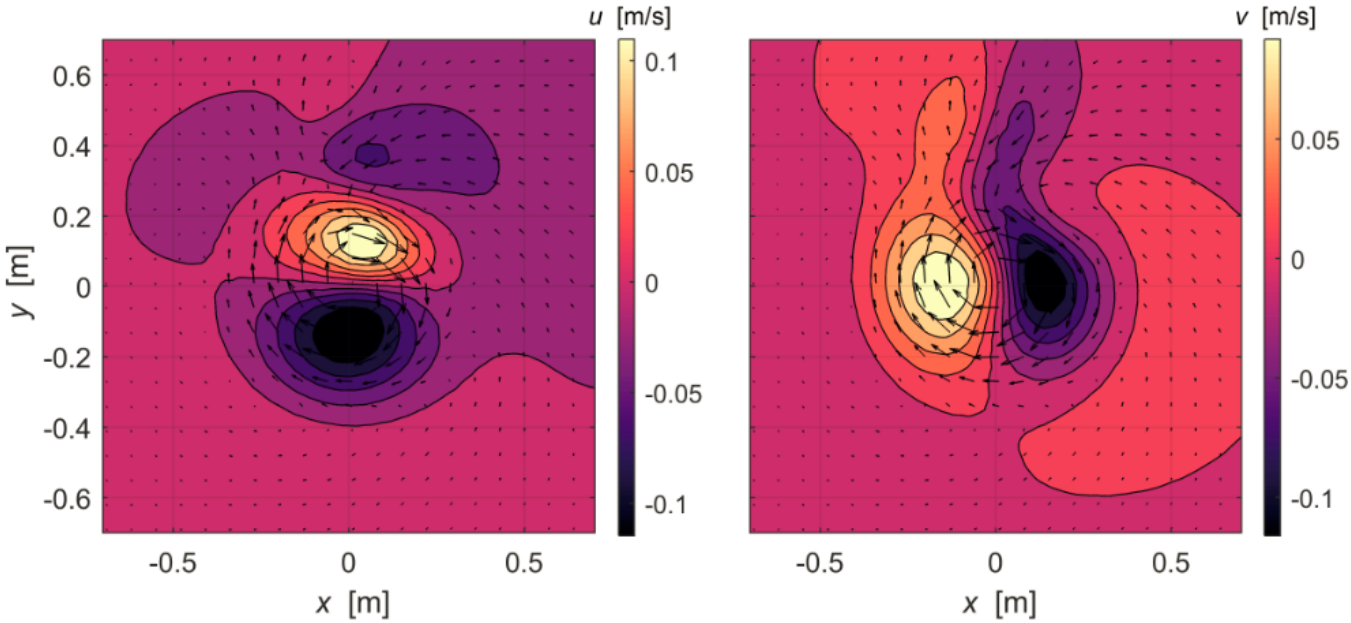

Figure 7 Velocity contour plots for *u* and *v* velocity components at 3*D* in the wake of the turbine.

The downstream turbine power and thrust coefficients C_p and C_T have been evaluated over the last 10 turbine rotations for all three setups when the system had reach a quasi-steady state (over the simulated time, the turbines had 33 complete rotations). The time evolution of both coefficients for the upstream and downstream turbine (for all three offset positions) is presented in Fig. 8 for one full rotation period.

The average values for each coefficient, and the absolute and relative amplitude of the fluctuation of each are presented in Table IX. First about the results, the upstream turbine performances are identical, within normal numerical uncertainty, compared to the results obtained for the single turbine simulations (0.5% difference for C_p; 0.08% for C_T). These observations are in line with what was observed by Jeffcoate *et al.* [4].

From Fig. 8 and Table IX, the 0*D* configuration leads to the lowest performance, followed by the 0.5*D* and 1*D* offsets. This is explained by the fact that with 0*D* offset, the downstream turbine essentially sees a highly turbulent flow already having a rotational component and an average velocity approximately 20 to 25% lower than the flow inlet velocity of 1 m/s (yet, the coefficients in this case are still dimensionalized using the constant inlet velocity). This clearly explains why the predicted C_p is 69% lower. This reduction goes down to 21% for the 0.5*D* offset configuration and a slight increase in C_p is observed (3%) when the downstream turbine is offset by 1*D*.

For C_T, the 0*D* configuration shows a reduction of 49% compared to the upstream turbine. The 0.5*D* configuration shows only a reduction of 15% while for 1*D*, C_T increases slightly by 2%.

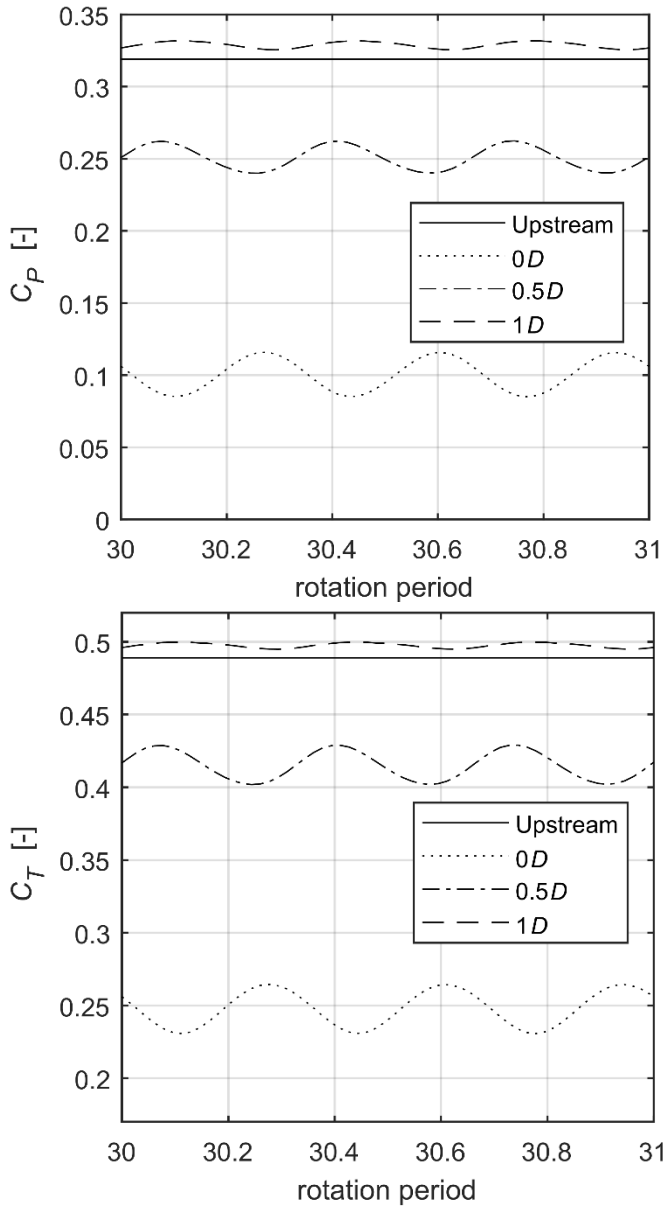

Figure 8 Numerical C_p and C_T over one rotation period at TSR = 4 for the upstream and downstream turbines for the three studied configurations.

Table IX
Upstream and Downstream Turbine Performance

	Upstream Turbine	Downstream Turbine Offset		
		0*D*	**0.5*D***	**1*D***
$\overline{C_p}$	0.3190	0.1004	0.2507	0.3288
Amplitude	-	0.0309	0.0230	0.0063
Relative Amplitude	-	30.77%	9.17%	1.91%
$\overline{C_t}$	0.4890	0.2478	0.4150	0.4975
Amplitude	-	0.0339	0.0280	0.0049
Relative Amplitude	-	13.6%	6.74%	0.98%

The increases shown in the 1*D* configuration are caused by the observed increase in wake velocity just outside of the central wake where a substantial velocity deficit is observed, as mentioned in the previous section.

Of particular interest from Fig. 8 is the oscillatory nature of both coefficients for the downstream turbine. The amplitude of the oscillation also being affected by the position of the downstream turbine in the wake of upstream one. All the time series show the same characteristics, with an oscillation period equal to 1/3rd of the rotation period of the turbine; although, the oscillation is out of phase for the three configurations. This is the result of the turbine blades experiencing the same flow but with a phase shift of ±1/3rd of the rotation period from each other. It appears that the oscillation is solely driven by the turbine rotation. The intensity of the time varying component of the incoming flow velocity in the wake is negligible compared to the local mean flow velocity and has no measurable effect on the downstream turbine performance.

The strongest amplitude of these oscillation is observed in the 0*D* configuration, with amplitudes decreasing with an increase in the offset of the downstream turbine. In the 0*D* configuration, C_p sees fluctuations of its value of over 30% above and below the average value. These variations in power extraction are happening rapidly, on a scale equal to 1/3rd of the rotation period, so less than 0.2 s for this configuration; they can potentially create issues in the energy producing and converting components of the turbine.

Even more important, from the loading/structural aspect of the blades, C_T sees fluctuations up to 13.6% around the average loading on the turbine, and its blade; again, also fluctuating over a short period. Therefore, the turbine blades will see varying local turbulent flow velocity during their rotation, which will lead to cyclical, and rapid, load variations on those blades.

The results from these simulations can be used to determine the extent of the loads, and fluctuation of those loads, on the turbine blades of the downstream turbine over time.

C. Downstream Turbine Blade Loading Analysis

In order to create a blade loading map for the downstream turbine and evaluate the load evolution along the blade span with respect to the blade location, the local thrust coefficient C_{T_l} is evaluated for each blade over a finite number of sections. The sections considered for this study are given in Fig. 9. Their respective areas are given in Table X. The local thrust coefficient is given by Eq. (14):

$$C_{T_l} = \frac{T_l}{\frac{1}{2}\rho_w A_s U_0^2} \tag{14}$$

where T_l is the local thrust computed at the n^{th} section and A_s is the total area of the n^{th} section.

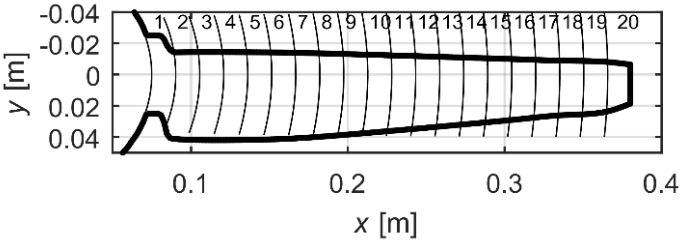

Figure 9 Turbine blade sections for discrete loading evaluation.

Table X
Blade Section Areas

Section	A_s [m²]	Section	A_s [m²]
1	2.55×10^{-3}	11	1.57×10^{-3}
2	2.05×10^{-3}	12	1.52×10^{-3}
3	2.03×10^{-3}	13	1.44×10^{-3}
4	2.00×10^{-3}	14	1.39×10^{-3}
5	1.95×10^{-3}	15	1.30×10^{-3}
6	1.90×10^{-3}	16	1.24×10^{-3}
7	1.82×10^{-3}	17	1.18×10^{-3}
8	1.77×10^{-3}	18	1.13×10^{-3}
9	1.73×10^{-3}	19	1.09×10^{-3}
10	1.62×10^{-3}	20	1.01×10^{-3}

The blade load spatial evolution is evaluated by making use of the local thrust coefficient C_{T_l}. The data gathered for all three turbine configurations, over 1,300 time steps, are used to compute the local thrust coefficient along the 20 sections of the blade span. These results are ordered with respect to the blade location on the swept area and are distributed over 72 sectors of 5° each which represent a full turbine rotation. This leads to an average of 34 values of C_{T_l} per blade section, per sector. From these results, the mean value of the local thrust coefficient $\overline{C_{T_l}}$ and the associated coefficient of variation CV, which is the standard deviation of the series divided by its mean and expressed as a percentage, are computed.

The results for $\overline{C_{T_l}}$ values are given in Fig. 10 and resulting CV values are presented in Fig. 11. Regarding the $\overline{C_{T_l}}$ distribution, the results are in line with the observation made earlier about the global performances. The $0D$ setup shows the most non-uniform blade load distribution. The most dramatic changes occur for the blade sections ranging from 10 to 20 (half of the blade nearer the tip) where the highest amplitude between the maximum and the minimum load for the same span location is observed. The maximum $\overline{C_{T_l}}$ is observed around section 18 with a value of 3.52. This value drops to a minimum of 1.42 for the same blade section later in its rotation. These maximum and minimum are indicated on Fig. 10 by a square and a triangular marker respectively. Therefore, the load on the same section of blade will change by a factor of 2 between maximum and minimum.

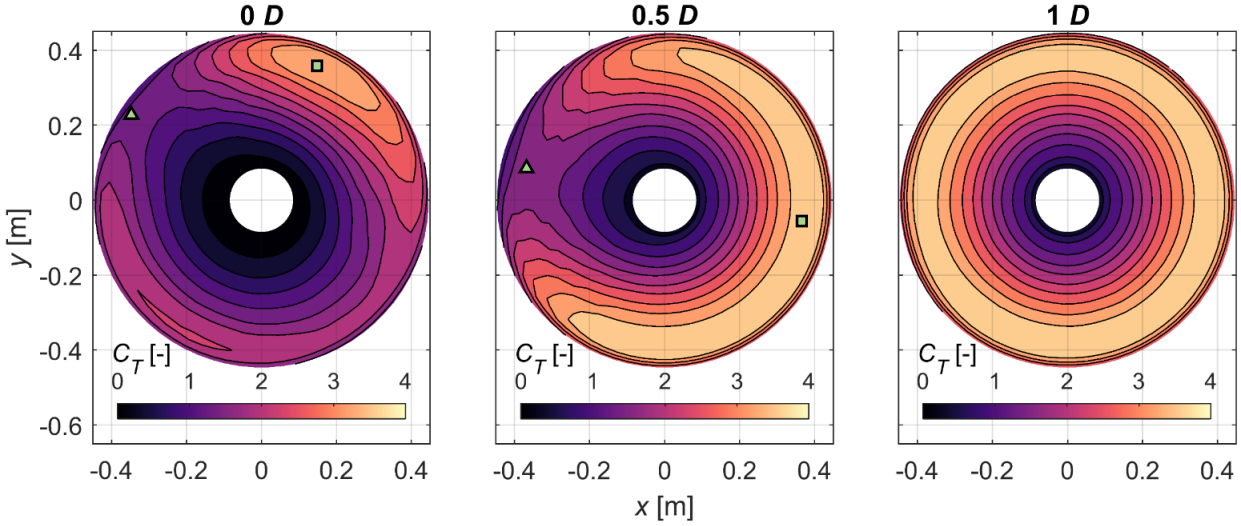

Figure 10 Values of $\overline{C_{T_l}}$ over the blade sections over their full rotation range for all three simulated configurations.

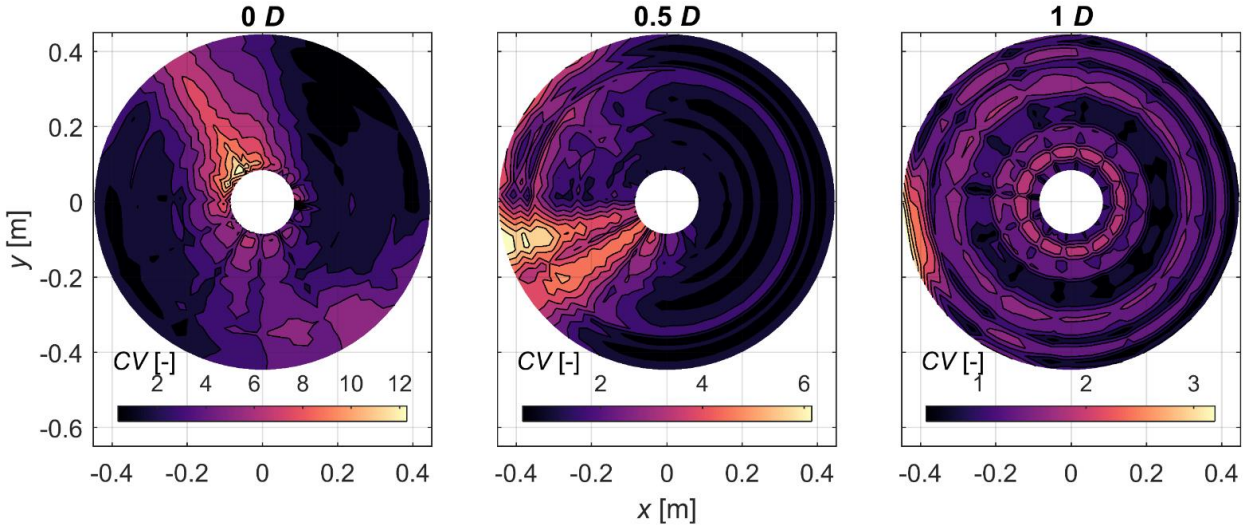

Figure 11 Values of *CV* over the blade sections over their full rotation range for all three simulated configurations.

For the 0.5D setup, the blades see less asymmetry and an overall higher C_{T_l} value. The blade load distribution is fairly constant over half of the swept area and sees a progressive decrease and increase on the West/Northwest sector when the blades rotate through the largest component of the upstream turbine wake. The maximum C_{T_l} value is 3.82, indicated by a square marker, while the lowest C_{T_l} value for the same span location is equal to 1.7 and is indicated by triangle marker.

The 1D setup experiences almost no asymmetry regarding the C_{T_l} distribution. The only marginal variation in the C_{T_l} values are barely visible for section 20 over the swept area.

Regarding the CV distribution in Fig. 11, the 0D setup experiences the strongest variability with the bulk of the variation located in the North/West sector of the swept area. The maximum value of CV is 13.3% and is located near the turbine hub. To a lesser extent, a reasonable amount of variation, with a value of CV between 3% to 6 % can also be observed in the South-Southeast region of the swept area around section 15 to 20. These areas roughly correspond to the one where lower value of C_{T_l} are observed.

For the 0.5D setup, the South/West sector of the swept area is the one which presents the highest values of CV with a maximum of 6.7% around sections 19 and 20. The upper left quarter of the swept area is also subject to some variation but to a lower level, with CV values ranging from 2.5% to 4.5% between sections 15 to 20. For the 1D setup, as expected, very small variations are observed, with a vast majority of the swept area having a CV value below 2%. The highest variation is observed for the West/Southwest sector around sections 19 and 20, where the CV reaches 3.4%.

VI. Conclusion

A fully transient numerical model of two three-bladed horizontal axis tidal turbines positioned one behind the other with a separation of 10D has been created and simulated. For a constant inlet velocity of 1 m/s, the results show that at a distance 10D behind the turbine, the wake still shows large areas of velocity deficit, up to 35% in velocity reduction compared to the inlet free-stream velocity. The wake also shows a large degree of asymmetry which will impact the overall performance of a second turbine downstream at this position.

When looking at the behaviour of a downstream turbine, it was found that C_p and C_T were both reduced, by up to 69% and 49% respectively when the downstream turbine is offset by less than a full turbine diameter. Both power and thrust are then subjected to large and rapid fluctuations which will have an impact on energy harvesting and overall blade loading leading to fatigue.

Looking specifically at the loading on the blades, it can vary by a factor of up to 2 during the blade rotation and changes in the amplitude of the load applied at the same location can fluctuate by more than 13%.

Acknowledgment

The authors are thankful to the French Embassy in Canada for the France Canada Research Fund (FCRF) award that supported this work, as well as to the Canadian Foundation for Innovation (CFI) for their financial assistance regarding the computing systems and the Faculty of Engineering at Dalhousie University.

References

[1] L. Hammar, S. Andersson, L. Eggertsen, J. Haglund, M. Gullstrom, J. Ehnberg, and S. Molander, "Hydrokinetic turbine effects on fish swimming behaviour," *PLoS One*, vol. 8, pp. e84141, 2013.

[2] T. Roc, D. Greaves, D.C. Conley, and M. Leybourne, "Optimising commercial-scale TEC arrays: genetic algorithm, Fractal & Eco-mimicry," in *10th European Wave and Tidal Energy Conference (EWTEC)*, 2013, 12 p.

[3] G. Bai, J. Li, P. Fan, and G. Li, "Numerical investigations of the effects of different arrays on power extractions of horizontal axis tidal current turbines," *Renewable Energy*, vol. 53, pp. 180-186, 2013.

[4] P. Jeffcoate, T. Whittaker, C. Boake, and B. Elsaesser, "Field tests of multiple 1/10 scale tidal turbines in steady flows," *Renewable Energy*, vol. 87, pp. 240-252, 2016.

[5] S.R. Turnock, A.B. Phillips, J. Banks, and R. Nicholls-Lee, "Modelling tidal current turbine wakes using a coupled RANS-BEMT approach as a tool for analysing power capture of arrays of turbines," *Ocean Engineering*, vol. 38, pp. 1300-1307, 2011.

[6] I. Masters, R. Malki, A.J. Williams, and T.N. Croft, "The influence of flow acceleration on tidal stream turbine wake dynamics: A numerical study using a coupled BEM–CFD model," *Applied Mathematical Modelling*, vol. 37, pp. 7905-7918, 2013.

[7] T. Leroux, N. Osbourne, J.M. McMillan, D. Groulx, and A.E. Hay, "Numerical Modelling of a Tidal Turbine Behaviour under Realistic Unsteady Tidal Flow," in *3rd Asian Wave and Tidal Energy Conference (AWTEC)*, 2016, 10 p.

[8] G. Currie, N. Osbourne, and D. Groulx, "Numerical Modelling of a Three-Bladed NREL S814 Tidal Turbine," in *3rd Asian Wave and Tidal Energy Conference (AWTEC)*, 2016, 10 p.

[9] N. Osbourne, D. Groulx, and I. Penesis, "3D Modelling of a Tidal Turbine - An Investigation of Wake Phenomena," in *11th European Wave and Tidal Energy Conference (EWTEC)*, 2015, 10 p.

[10] D.A. Doman, R.E. Murray, M.J. Pegg, K. Gracie, C.M. Johnstone, and T. Nevalainen, "Tow-tank testing of a 1/20th scale horizontal axis tidal turbine with uncertainty analysis," *International Journal of Marine Energy*, vol. 11, pp. 105-119, 2015.

[11] I. Afgan, J. McNaughton, S. Rolfo, D.D. Apsley, T. Stallard, and P. Stansby, "Turbulent flow and loading on a tidal stream turbine by LES and RANS," *International Journal of Heat and Fluid Flow*, vol. 43, pp. 96-108, 2013.

[12] M. Fleisinger, M. Vesenjak, and M. Hriberšek, "Flow Driven Analysis of a Darrieus Water Turbine," *Strojniški vestnik – Journal of Mechanical Engineering*, vol. 60, pp. 769-776, 2014.

[13] J.H. Lee, S. Park, D.H. Kim, S.H. Rhee, and M.-C. Kim, "Computational methods for performance analysis of horizontal axis tidal stream turbines," *Applied Energy*, vol. 98, pp. 512-523, 2012.

[14] F. Menter, *Zonal Two Equation k-w Turbulence Models For Aerodynamic Flows*, in 23rd Fluid Dynamics, Plasmadynamics, and Lasers Conference, American Institute of Aeronautics and Astronautics,1993.

[15] P.J. Roache, *Verification and Validation in Computational Science and Engineering*, Albuquerque, NM: Hermosa Pub, 1998.

[16] I.B. Celik, U. Ghia, P.J. Roache, C.J. Freitas, H. Coleman, and P.E. Raad, "Procedure for Estimation and Reporting of Uncertainty Due to Discretization in CFD Applications," *Journal of Fluids Engineering*, vol. 130, pp. 078001, 2008.

[17] P.J. Roache, "Perspective: A Method for Uniform Reporting of Grid Refinement Studies," *Journal of Fluids Engineering*, vol. 116, pp. 405-413, 1994.

[18] N. Osbourne, "3D Modelling of a Tidal Turbine - A Numerical Investigation of Wake Phenomena," MASc thesis, Mechanical Engineering, Dalhousie University, Halifax, NS, 2015

[19] S. Le DizÈS and A. Verga, "Viscous interactions of two co-rotating vortices before merging," *Journal of Fluid Mechanics*, vol. 467, pp. 389-410, 2002.